Characterization of TMEM43 as a novel ion channel

Minwoo Wendy Jang[1], Joungha Won[1], Young-Eun Han[1,#], Jae-Hun Lee[1], Ah-reum Han[2], Ho Min Kim[2,3], and C. Justin Lee[1*]

[1]Center for Cognition and Sociality, Institute for Basic Science (IBS), Daejeon 34126, Republic of Korea, [2]Center for Biomolecular and Cellular Structure, Institute for Basic Science (IBS), Daejeon 34126, Republic of Korea, [3]Graduate School of Medical Science and Engineering, Korea Advanced Institute of Science and Technology (KAIST), Daejeon 34141, Republic of Korea, [#]Current address: Brain Science Institute, Korea Institute of Science and Technology (KIST), Seoul, 02792, Republic of Korea

[*]Correspondence: cjl@ibs.re.kr

Abstract

TMEM43 is a transmembrane protein with four transmembrane (TM) domains. The *TMEM43* gene has been reported to play supportive but critical roles in many human diseases, such as cancer, arrhythmogenic right ventricular cardiomyopathy (ARVC), and auditory neuropathy spectrum disorder (ANSD). However, the direct characterization of the TMEM43 protein is missing. In this study, we examined the function of TMEM43 *in vitro*. Heterologous expression of TMEM43 demonstrated that TMEM43 is permeable to Na^+, K^+, and Cs^+ ions, indicating that TMEM43 is a nonselective cation channel. The TMEM43-mediated current decreased gradually with lowering external solution pH, further characterizing TMEM43 as an external-pH sensing channel. Utilizing the endogenous cysteine residue at TM3, we could predict that the pore-forming residue of TMEM43 lies near TM3 and Loop2 domain. Importantly, stochastic channel openings from the lipid bilayer-reconstituted purified TMEM43 protein were observed, strengthening the proposal of TMEM43 as an ion channel. Lastly, the heterologous expression of *TMEM43*-p.(Arg372Ter) resulted in a loss of channel activity in a dominant-negative fashion, as in the hearing loss phenotype in humans. These results together disclose the molecular and functional properties of TMEM43 and identify TMEM43 as a novel ion channel. The physiological identity of TMEM43 provided in this study will promote future research on TMEM43-related diseases.

Keywords

TMEM43, Ion channel, Nonselective cation channel, Acid-sensing channel

Introduction

The role of *the TMEM43* gene has been implicated in human diseases such as glioblastoma (1), pancreatic cancer (2), arrhythmogenic right ventricular cardiomyopathy (ARVC) (3, 4), and auditory neuropathy spectrum disorder (ANSD) (5). Mechanistically, TMEM43 interacts with the scaffold protein CARMA3 and its associating complex to induce downstream NF-κB activation and plays a critical role in controlling brain tumor progression (1). TMEM43 is also known to stabilize PRPF3 and regulate RAP2B/ERK axis, accelerating the progression of pancreatic cancer (2). In the heart, the *TMEM43*-p.(Ser358Leu) mutation increases the stiffness of the cell nucleus, which might lead to massive loss of cardiomyocytes (6) while altering intercalated disc protein expression, disturbing gap junction transfer, and reducing conduction velocity in cardiac cell lines (7). In the cochlea, TMEM43 was shown to interact with predominant gap junction channels Connexin 26 (Cx26) and Cx30 to mediate the large potassium (K^+) conductance current in the cochlear glia-like supporting cells (5). This K^+ conductance was significantly reduced when the *TMEM43*-p.(Arg372Ter) variant was introduced, leading to progressive hearing loss (5). In addition to the clinical studies, *in vitro* and *ex vivo* studies also demonstrate that TMEM43 interacts with secondary proteins. For instance, TMEM43 interacts with emerin and A- and B-type lamins in undifferentiated C2C12 cells (8) and with one of the two-pore-domain potassium (K2P) channels, KCNK3 (TASK-1) in the cochlea (9).

Although TMEM43 has been reported to play supportive but critical roles in many human diseases, direct characterization of TMEM43 protein itself is missing. The involvement of TMEM43 in cardiac rhythmicity (7), gap junction-mediated dye diffusion (7), and passive conductance current (5) imply the possibility of TMEM43 to be functioning as an ion conductor. In this study, we disclose TMEM43 as a new class of pH-sensitive and nonselective cation channel and provide a putative channel pore domain.

Results

An ion channel must traffic to the cell plasma membrane to elicit channel currents. We have previously shown that TMEM43 protein localizes to the cell surface by biotinylation assay and immunostaining (5). To ensure the TMEM43 localization and topology in this study, we tagged Myc and FLAG at the N-terminus and C-terminus of TMEM43, respectively (**Figure 1A**), and performed immunocytochemistry with or without cell permeabilization in the heterologous expression system. As expected, both Myc and FLAG signals were detected from TMEM43-expressing cells in cell permeabilization and non-permeabilization conditions (**Figure 1B**). These results support the membrane trafficking property of TMEM43. After confirming the membrane localization of TMEM43, we examined single-channel activities from purified TMEM43 protein. Evident voltage-dependent channel openings and closings were observed in the lipid bilayer-reconstituted purified TMEM43 protein (**Figure 1C-E**). TMEM43 was silent at a holding potential of 0 mV, but the channel activity increased with growing holding potentials in both directions (**Figure 1C, D**). The direction of the TMEM43-induced current switched at 0 mV, indicating the reversal potential of TMEM43 at around 0 mV. These membrane trafficking properties and stochastic channel openings observed in TMEM43 are typical features of an ion channel.

To investigate the ion channel characteristics of TMEM43, we heterologously expressed TMEM43 in CHO-K1 cells and measured its membrane currents under a voltage clamp. Compared to naïve CHO-K1 cells, TMEM43-transfected CHO-K1 cells displayed significantly higher amplitude of both inward and outward passive membrane currents with an average reversal potential of -15.5 mV after junction potential correction **(Figure 2A, C, D).** Furthermore, TMEM43-induced current showed a doubly rectifying I-V curve, resembling the voltage-dependent probabilistic channel openings measured from the purified TMEM43 protein (**Figure 1C**). The inward current mediated by TMEM43 was due to an influx of sodium ions (Na^+) based on the observation that the substitution of Na^+-free external solution eliminated the inward current **(Figure 2B, C)** with a significant shift of reversal potential **(Figure 1D)**. The outward current was carried by potassium ions (K^+), as evidenced by the observation that the outward current was absent with an elimination of intracellular K^+ **(Figure 1B, C)** or by cesium ions (Cs^+) as the current was present with a substitution of intracellular Cs^+ **(Figure 3A-F)**. These results indicate that TMEM43 is a nonselective cation channel with permeability to cations such as Na^+, K^+, and Cs^+. As expected, TMEM43-mediated current was significantly and potently blocked by well-known nonselective cation channel blocker $GdCl_3$ (10), with a half-maximal inhibition of 0.840 μM **(Figure 1E, F)**. In addition, TMEM43-mediated current was not affected by either intracellular chloride ion (Cl^-) **(Figure 3A-C)** or calcium ion (Ca^{2+}) **(Figure 3D-F)** substitution, indicating that TMEM43 is neither an anion channel nor a Ca^{2+}-activated channel. It is noteworthy that TMEM43-mediated current was inhibited dose-dependently by gradually lowering the extracellular pH from 8 to 5.5 with half-maximal inhibition at pH 6.495 **(Figure 2G, H)**, elucidating TMEM43 as a pH-sensitive channel. However, the change in the intracellular pH did not affect the channel current **(Figure 3G-H).** Altogether, these results define TMEM43 as an external pH-sensitive and nonselective cation channel.

The TMEM43-mediated current increased dramatically in the hyperpolarizing potentials, negative to -100 mV (**Figure 1C, Figure 4A**). The current-voltage (I/V) curve from TMEM43-expressing cells highly resembled the current measure from inwardly rectifying potassium channel (K_{ir}) channel-expressing cells (11, 12). Therefore, we checked if TMEM43 shares the characteristics of K_{ir} channels or if TMEM43 interacts with K_{ir} channels. We found that treating barium (Ba^{2+}), a selective blocker of K_{ir} channels (13), did not interrupt the TMEM43-induced large inward current at hyperpolarizing potentials (**Figure 4A, B**). We next tested if TMEM43 interacts with K_{ir}4.1, a dominant K_{ir} channel in the central nervous system to regulate K^+ homeostasis (14, 15). The co-immunoprecipitation assay revealed that TMEM43 does not interact with K_{ir}4.1 (**Figure 4C**). These results indicate that the large inward currents at the hyperpolarizing potentials can be identified as a TMEM43-induced current independent of K_{ir} channels.

To determine the putative pore region of TMEM43 based on the membrane topology of TMEM43 (**Figure 1A**), we performed the substituted-cysteine accessibility method (SCAM) (16) using MTSES (Sodium (2-Sulfonatoethyl) methanethiosulfonate) as a reducing agent. MTSES binds strongly with the sulfhydryl groups of cysteine to block channel current if cysteine lies near the channel pore region (16, 17). The TMEM43 wild type (WT) contains only one cysteine residue (Cys354) at the transmembrane domain (TM) 3. Surprisingly, treating 100 μM MTSES to TMEM43-expressing cell abated channel current by about 40 % **(Figure 5A, C)**. This MTSES blockage disappeared when the endogenous cysteine at Cys354 was mutated to alanine p.(Cys354Ala) **(Figure 5B, C),** indicating that Cys354 is near or at the pore region of TMEM43. Furthermore, the reversal potential was significantly shifted after MTSES treatment in TMEM43 WT but not in TMEM43-p.(Cys354Ala) **(Figure 5D)**, indicating that the mutation caused a change in ion selectivity. To further narrow the pore region, we thoroughly examined the Loop2, which lies between TM2 and the cysteine-containing TM3. The deletion mutation of Loop2 (ΔLoop2) resulted in a complete loss of TMEM43-mediated current (**Figure 5E-G**). To check if the loss of current was due to a reduction in surface trafficking of TMEM43, we performed a biotinylation assay. We found that TMEM43-ΔLoop2 showed intact surface trafficking (**Figure 5H**), indicating the possibility that the Loop2 domain constitutes a putative pore domain of TMEM43. Next, we substituted each of the ten amino acids at the Loop2 domain to cysteine in the TMEM43-p.(Cys354Ala) background to perform the SCAM experiment (**Figure 5I-K**). MTSES block percentage plot showed an 'M' shaped distribution with two maximal block percentages near two negatively charged aspartic acid residues of p.(Asp335Cys) and p.(Asp342Cys) with a middle dip at the kink-forming proline residue of p.(Pro338Cys) (**Figure 5K**). The SCAM results propose a putative model of the TMEM43 pore structure with two charged residues per subunit to form a pore (**Figure 5K, inset**). These results strengthen the idea that TMEM43 is a *bona fide* ion channel with channel pore residues near the Loop2 domain, lining between TM2 and TM3.

The genetic variants of the human *TMEM43* gene have been highlighted in clinical studies. The *TMEM43*-p.(Arg372Ter) variant causes ANSD (5) and the *TMEM43*-p.(Ser385Leu) variant leads to ARVC in humans (3, 4). Therefore, we investigated whether TMEM43-mediated current is disturbed in the two *TMEM43* variants in the heterologous expression system. Whole-cell voltage clamp experiments revealed that *TMEM43*-p.(Arg372Ter) variant resulted in an abolishment of both inward

and outward TMEM43-mediated current **(Figure 6A, B, D)**, clearly documenting the pathogenic effect of the variant on the channel function. Furthermore, co-expression of *TMEM4*-WT and p.(Arg372Ter) variant showed a significantly lower current than that of WT but comparable to that of mutant, especially at -100 mV, indicating that the pathogenic effect of the variant in TMEM43 is dominant-negative **(Figure 6c, D)**. This result is compatible with the *TMEM43*-p.(Arg372Ter) autosomal dominant inheritance in humans as previously shown by linkage analysis and whole exome sequencing (5). In contrast, *TMEM43*-p.(Ser358Leu) did not cause any impairment of the nonselective cation current (**Figure 6E-G**), raising a possibility that the p.(Ser358Leu) and the p.(Arg372Ter) variants manifest profoundly different pathogenic mechanisms.

Discussion

TMEM43 was initially identified in the inner nuclear membrane (8) and *in silico* as one of the 368 transmembrane proteins with unknown function (TMEM) (18). A few unknown TMEMs have been identified as ion channels, including ANO1 (TMEM16A) as a Ca^{2+}-activated anion channel (19) and TENTONIN3 (TMEM150C) as a mechanosensitive cation channel (20). Although pathological functions of TMEM43 have been implicated in many human diseases, the characterization of the TMEM43 protein itself is missing in the field. It has been demonstrated that disruption of TMEM43 protein in the cochlea by gene-silencing, introducing the genetic variant *TMEM43*-p.(Arg372Ter), and interrupting TMEM43-interacting proteins such as Cx26, Cx30, and TASK-1, all resulted in the loss of K^+ conductance current in the cochlear glia-like supporting cells (5, 9). We got insight from the previous studies and hypothesized that TMEM43 might encode a new class of ion channels. In this study, we utilized purified TMEM43 protein and heterologous gene expression system combined with intensive electrophysiology and identified TMEM43 as an acid-sensing cation channel. Based on the predicted TMEM43 topology, we further characterized the putative channel pore domain to be including the Loop2 domain. Future research on TMEM43 protein, such as the cryo-EM-based protein structure reconstruction, would reveal channel pore domain, pH-sensing domain and protein-protein interaction domain.

It is interesting to note the different outcomes of *TMEM43*-p.(Arg372Ter) and *TMEM43*-p.(Arg358Leu) variants in the heterologous system. This difference could come from the presence of the TM4 domain, as the nonsense p.(Arg372Ter) variant results in truncation of the TM4 domain, while the missense p.(Arg358Leu) variant still retains TM4. Lack of the TM4 may decompose TMEM43 oligomerization or ion-conducting passage, resulting in loss of channel currents. This conflicting result suggests that the p.(Arg372Ter) and p.(Ser358Leu) variants of *TMEM43* exert a completely different pathophysiological mechanism, leading to the pleiotropy of this gene. Since the p.(Arg372Ter) and p.(Ser358Leu) variants caused pathology in the cochlea and the heart, respectively, different actions of secondary proteins and post-translational modifications can occur in different organs. Therefore, further studies using TMEM43 null knock-out mice are required to understand TMEM43 pathology comprehensively.

In conclusion, we have identified and characterized TMEM43 as a novel ion channel. Furthermore, by providing the electrophysiological properties of TMEM43 *in vitro*, this study will expedite further studies in finding a therapeutic target for TMEM43-related pathology and disclosing the unidentified role of TMEM43 *in vivo*.

Methods

Plasmids

TMEM43 Human Tagged ORF Clone (NM_024334.2) was purchased from OriGene (RC200998) and cloned into CMV-MCS-IRES2-EGFP vector using BglII/XmaI sites. *TMEM43* variants, including *TMEM43*-p.(Arg372Ter), *TMEM43*-(p.Ser358Leu), and site-directed mutations were obtained by performing oligonucleotide-directed mutagenesis using the EZchange site-directed mutagenesis kit (EZ004S, Enzynomics) and cloned into CMV-MCS-IRES2-EGFP or CMV-MCS-IRES2-tdTomato vector using BglII/XmaI sites. KCNK3 (Myc-DDK-tagged) (TASK-1) (NM_002246.3) was purchased from OriGene (RC215155) and cloned into IRES2 vector using BglII/XhoI sites, and K_{ir}4.1 (NM_031602) was purchased from addgene (52874) and cloned into IRES2 vector using XhoI/SalI sites.

Heterologous expression of TMEM43 in mammalian cell lines

Human embryonic kidney (HEK) 293T cells and Chinese hamster ovary (CHO)-K1 cells were each purchased from ATCC (CRL-3216) and the Korean Cell Line Bank (10061, Seoul National University), respectively. All cell lines have been tested for mycoplasma contamination. Cell lines were cultured in DMEM (10-013, Corning) for HEK293T cells and Ham's F12 medium (21127-022, Gibco) for CHO-K1 cells, which were supplemented with 10 % heat-inactivated fetal bovine serum (10082-147, Gibco) and 10,000 units/ml penicillin-streptomycin (15140-122, Gibco) at 37 ˚C in a humidified atmosphere of 95 % air and 5 % CO_2. Transfection of expression vectors was performed with Effectene Transfection Reagent (Effectene, 301425, Qiagen), according to the manufacturer's protocol. One day before performing whole cell patch experiments, CHO-K1 cells were transfected with plasmid DNA 1 μg per 35 mm dish. The ratio of DNA to Effectene Reagent is 1:10.

Immunocytofluorescence on heterologous system

For immunocytochemistry, pCMV-*TMEM43*-IRES2-EGFP were transfected into HEK293T cells one day before staining. Cells were fixed in 4 % paraformaldehyde for 10 minutes at room temperature and washed 3 times with PBS. The permeabilized group contained 0.3 % Triton X-100 in the blocking solution with 2 % goat serum and 2% donkey serum, but the impermeabilized group excluded Triton X-100 in the blocking solution. Cells were incubated with mouse anti-Myc (1:500, 2276, cell signaling) and rabbit anti-FLAG (1:500, 2368, cell signaling) at 4°C overnight. After washing, donkey anti-mouse Alexa 594 (1:500, Jackson, 715-585-150) and donkey anti-rabbit Alexa 647 (1:500, Jackson, 711-605-152) were added and incubated for 2 hours at room temperature. The cells were washed 3 times, mounted on slide glasses, and observed under a Zeiss confocal microscope (LSM900).

Protein purification

TMEM43-EGFP-thrombin-twinstrep (1 μg) was expressed in Expi293 cell line ($3X10^6$ cells/ml, 200 ml in 1 L flask) using ExpiFectamine™ 293 Transfection Kit (Gibco, A14524). After 48 hours, cells were lysed using a sonicator, and cell debris was removed by 4000 rpm, 30 min, 4°C centrifugation. Then,

150000 g, 1 hour, 4°C ultra-centrifugation was done to separate membrane proteins. The membrane pellet was mechanically homogenized and solubilized for 2 hours at 4°C in a buffer that contained 250 mM NaCl, 50 mM HEPES (pH 7.5) in 1% n-Dodecyl-β-D-Maltoside Lauryl Maltoside Dodecyl 4-O-α-D-Glucopyranosyl-β-D-Glucopyranoside (DDM) (Antrace, 69227-93-6) and 0.1% Cholesteryl Hemisuccinate Tris Salt (CHS) (Antrace, 102601-49-0). Insoluble material was removed by ultra-centrifugation (150000 g, 1 hour, 4°C). Finally, TMEM43 protein was filtered using Strep-tactin resin (IBA, 2-1201-025) and eluted with 0.02% DDM and 10 mM D-biotin (IBA, 2-1000-005).

Chemicals

Gadolinium chloride ($GdCl_3$) was purchased from Sigma-Aldrich (G7532); Barium chloride ($BaCl_2$) was purchased from Sigma-Aldrich (B0750); Sodium (2-Sulfonatoethyl) methanethiosulfonate (MTSES) was purchased from Toronto Research Chemicals (S672000).

Electrophysiological recording in CHO-K1 cells

Current-voltage (I–V) curves were recorded from CHO-K1 cells one day after plasmid DNA transfection. I–V curves were established by applying 1-second duration voltage ramps descending from +100 mV to -100 mV, with -60 mV holding potential. Transfected CHO-K1 cells were distinguished by fluorescence using an Olympus IX71 inverted microscope. Recording pipettes were fabricated from borosilicate glass capillaries (TW150F-4, World Precision Instruments) using a P-97 Flaming/Brown micropipette puller (Sutter Instruments). The standard bath solution contained (in mM): 150 NaCl, 3 KCl, 2 CaCl2, 2 MgCl2, 10 HEPES, and 5.5 D-glucose (pH 7.4 was adjusted with NaOH). For measuring potassium currents, recording electrodes (5–8 MΩ) were filled with (mM): 126 KOH, 126 Gluconate, 5 HEPES, 0.5 $MgCl_2$, and 10 BAPTA (pH adjusted to 7.3 with KOH). To measure sodium currents, recording electrodes (5–8 MΩ) were filled with (mM): 126 NMDG, 126 Gluconate, 5 HEPES, 0.5 $MgCl_2$, and 10 BAPTA. Then, the bath solution was shifted from standard buffer to NMDG buffer (in mM: 120 NMDG-Cl, 10 HEPES, 3 KCl, 2 $CaCl_2$, 2 $MgCl_2$, and 5.5 glucose, pH 7.3). For measuring cesium current and calcium-dependent current, recording electrodes (5–8 MΩ) were filled with (mM): 106 CsCl, 20 TEA-Cl, 5 HEPES, 0.5 $MgCl_2$, 10 BAPTA, and 0 and 9.95 $CaCl_2$ to make 0 µM and 10 µM Ca^{2+} (pH adjusted to 7.3 with CsOH). For measuring chloride currents, recording electrodes (5–8 MΩ) were filled with (mM): 20 TEA-Cl, 5 HEPES, 0.5 $MgCl_2$, 10 BAPTA, and each 106 gluconate and 106 CsCl to make 1 mM Cl^- and 127 mM Cl^- (pH adjusted to 7.3 with CsOH). To measure the external pH-dependent current, HEPES buffer was made and adjusted initially to pH 5 with NaOH, and pH was increased serially by adding NaOH. To measure the internal pH-dependent current, the pH of the K-gluconate internal solution was serially adjusted with KOH from pH 5 to 8. Whole-cell membrane currents were amplified by the Axopatch 200A, and data acquisition was controlled by pCLAMP 10.2 software (Molecular Devices). The Digidata 1322A interface was used to convert digital-analog signals between the amplifier and the computer. Data were sampled at 10 kHz and filtered at 2 kHz. Cell membrane capacitance was measured using the 'membrane test' protocol built into pCLAMP. All experiments were conducted at a room temperature of 20-22°C. All I-V curves were constructed without liquid junction potential correction. However, the

reversal potentials were calculated by subtracting the measured liquid junction potential (-14 mV) from the observed values.

Single-channel recordings

The Orbit mini apparatus (Nanion, Germany, horizontal planar lipid bilayer system) was used to record single-channel activities. The Orbit mini is a miniaturized bilayer workstation that simultaneously enables recording from four artificial lipid bilayers. The recordings were done in a symmetrical 140 mM KCl (pH 7.2) solution at room temperature. DPhPC (1 mg/ml) dissolved in Octane was used to paint a bilayer over the four 100 µm diameter wells in a Meca4 chip (Nanion). Purified TMEM43 protein in DDM detergent (0.02 %) was loaded into the bath solution after forming the bilayers.

Cell surface biotinylation, co-immunoprecipitation, and western blot.

For biotinylation, plasmid vectors were transfected into HEK293T cells 1 day before the experiment day. Transfected cells were washed three times with PBS, and cell surface-expressed proteins were biotinylated in PBS containing Ez-link sulfo-NHS-LC-Biotin (21335, Thermo) for 30 minutes. After biotinylation, cells were washed with quenching buffer (100 mM glycine in PBS) to remove excess biotin and washed three times with PBS. The cells were then lysed and incubated with high-capacity NeutrAvidin-Agarose Resin (29204, Thermo). After three washes with lysis buffer, bound proteins are eluted by the SDS sample buffer and subjected to western blot analysis. Rabbit anti-TMEM43 polyclonal (1:250, NBP1-84132, Novus) and rabbit anti-β-Actin (1:1000, 4970L, Cell signaling) were used as primary antibodies, and donkey anti-rabbit HRP (NA9340, Amersham) was used as a secondary antibody. For co-immunoprecipitation, cell lysates were prepared in a buffer containing 50 mM Tris-HCl (pH 7.5), 150 mM NaCl, 1 % NP-40, 10 mM NaF, and a protease and phosphatase inhibitor cocktail. Equal amounts of precleared cell lysates were incubated with rabbit anti-TMEM43 polyclonal (1 µg, NBP1-84132, Novus) overnight at 4°C. Protein A/G-Agarose beads (Thermo Fisher Scientific) were added to the mixtures and further incubated for 2 hours, followed by a wash with lysis buffer. Bound proteins were eluted from the beads with SDS-PAGE sample buffer, and western blotting was performed with mouse anti-TASK-1(KCNK3) (1:250, NBP2-42202, Novus) or rabbit anti-K_{ir}4.1 (1:250, APC-035, Alomone Labs).

Data analysis and statistical analysis

Off-line analysis was carried out using Clampfit version 10.6 and GraphPad Prism version 9 software. When comparing two samples, the significance of data was assessed by Student's two-tailed unpaired t-test when samples showed normal distribution and assessed by the Mann-Whitney test when samples did not pass the normality test. Samples that passed the normality test but not the equal variance test were assessed with Welch's correction. Comparing more than 2 samples were analyzed using one-way ANOVA with Tukey's post-hoc test when data passed the normality test and Kruskal-Wallis test with Dunn's post-hoc test when data did not pass the normality test. Significance levels were given as: N.S. $P>0.05$, *$P<0.05$, **$P<0.01$, ***$P<0.001$ and #$P<0.0001$ in all figures.

Acknowledgments

This research was supported by Institute for Basic Science (Grant/Award Number: IBS-R001-D2) to C. Justin Lee.

Figure legends

Figure 1. Membrane trafficking and single-channel activities of TMEM43

(A) Illustration of TMEM43 topology based on hydrophobicity analysis. Myc is tagged at the N-terminus, and FLAG is tagged at the C-terminus of TMEM43. **(B)** Immunostaining result of TMEM43-expressing HEK293T cells with and without cell permeabilization. Cells were double stained with Myc and FLAG antibodies. **(C)** Stochastic channel gating of purified TMEM43 protein in different holding potentials. Closed states are indicated in the black bar with the letter C, and maximum open states are indicated in the pink bar with the letter O. **(D, E)** Distribution of amplitude **(D)** and dwell time **(E)** from open states.

Figure 2. TMEM43 is a nonselective cation channel with external pH sensitivity

(A) Representative current traces from naïve (black) and *TMEM43* (Pink) transfected CHO-K1 cells. Current traces were elicited by 1-second ramps descending from +100 mV to -100 mV. Inset: a schematic diagram of patch-clamped cells. **(B)** Representative current traces from *TMEM43* transfected cells in the presence (green) and absence (grey) of external Na^+. The patch pipette is filled with N-methyl-D-glucamine (NMDG) gluconate, free of Na^+ and K^+. **(C)** Summary bar graph of currents plotted at -100 mV (I_{-100mV}) and +100 mV (I_{+100mV}) for each condition in **(A, B)**. **(D)** Reversal potential (V_{rev}) of respective conditions in **(A, B)** after junction potential correction. **(E)** Representative whole-cell I-V curves from cells expressing *TMEM43* before (black) and after (pink) $GdCl_3$ treatment (100 μM shown), measured in the same cell. **(F)** Dose-response curve for $GdCl_3$ blocking TMEM43 current. **(G)** Representative current-voltage relationship in *TMEM43*-expressing cells with gradually decreasing external solution pH in the same cell. (**H**) Dose-dependent inhibition of external solution acidic pH on TMEM43-mediated current. Data is presented as averaged % remaining currents ± SEM plotted at -100 mV.

Figure 3. TMEM43 is not an anion channel nor a Ca^{2+}-activated channel

(A, B) Representative whole-cell I-V curves from HEK293T cells expressing TMEM43 with 127 mM [Cl^-] **(A)** and 1 mM [Cl^-] in the internal pipette solution **(B)**. **(C)** Summary bar graph of **(A, B)**. **(D, E)** Representative current traces from TMEM43-expressing cells with 10 μM [Ca^{2+}] **(D)** and 0 μM [Ca^{2+}] **(E)** in the patch pipettes. **(F)**, Summary bar graph of **(D, E)**. **(G, H)** Representative current-voltage relationship in TMEM43-expressing cells with internal pipette solution pH 7.3 **(G)** and pH 5 **(H)**. **(I)** Summary bar graph of TMEM43 currents measured with different pH in the internal solutions.

Figure 4. TMEM43 induces current independent of K_{ir} channels

(A) Representative whole-cell I-V curves from naïve CHO-K1 cell and *TMEM43*-expressing cell before (pink) and after (black) $BaCl_2$ treatment (100 μM shown). **(B)** Summary bar graph of currents plotted at -150 mV (I_{-150mV}) and +50 mV (I_{+50mV}) for each condition in **(A)**. **(C)** Co-immunoprecipitation results of TMEM43 expressed with TASK-1 and K_{ir}4.1. Cell lysates were immuno-pulled with an anti-TMEM43 antibody and blotted with TASK-1 and K_{ir}4.1 antibodies. TASK-1 was shown as a positive control.

Figure 5. The putative channel pore domain of TMEM43 consists Loop2 domain

(A, B) Representative I-V curves before (pink) and after (black) MTSES (100 μM) treatment in *TMEM43* WT-expressing **(A)** and *TMEM43*-p.(Cys354Ala)-expressing **(C)** cells. Raw traces are plotted in lower panels. **(C)** Average current block percentage by MTSES treatment measured from **(A, B)**. **(D)** Average reversal potential measured from **(A, B)**. **(E, F)** Representative I-V curves of *TMEM43* WT **(E)** and Loop2 truncated (ΔLoop2) **(F)** -expressing cells. **(G)** The average current amplitude of **(E, F)**. **(H)** Cell surface biotinylation assay in *TMEM43* WT and ΔLoop2 transfected HEK293T cells blotted with TMEM43 antibody. Naïve HEK293T cells and TMEM43-p.(Arg372Ter)-expressing cells were used as negative controls. **(I, J)**, Representative I-V curves before (pink) and after (black) 100 μM MTSES treatment of *TMEM43*-p.(Asp335Cys/Cys354Ala) transfected **(I)** and *TMEM43*-p.(Asp342Cys/Cys354Ala) transfected **(J)** cells. Raw traces are plotted in lower panels. **(K)** Average MTSES block percentage measured in cysteine substituted residues at Loop2 domain in p.(Cys354Ala) background. The proposed TMEM43 structure with putative channel pore is shown in the upper panel.

Figure 6. TMEM43-mediated currents with genetic variants

(A-C) Representative whole-cell I-V curves from cells transfected with *TMEM43* WT **(A)**, *TMEM43*-p.(Arg372Ter) **(B)**, or *TMEM43* WT and *TMEM43*-p.(Arg372Ter) (1:1) **(C)**. Insets: fluorescent images of a CHO-K1 cell expressing both TMEM43 WT (GFP) and TMEM43-p.(Arg372Ter) (tdTomato). **(D)** Summary bar graph of currents from **(A-C)**. **(E-F)** Representative whole-cell I-V curves from cells transfected with *TMEM43* WT **(E)** and *TMEM43*-p.(Ser358Leu) **(F)**. **(G)** Averaged current amplitudes from **(E, F)**.

References

1. C. Jiang *et al.*, TMEM43/LUMA is a key signaling component mediating EGFR-induced NF-kappaB activation and tumor progression. *Oncogene* **36**, 2813-2823 (2017).
2. J. Li *et al.*, TMEM43 promotes pancreatic cancer progression by stabilizing PRPF3 and regulating RAP2B/ERK axis. *Cell. Mol. Biol. Lett.* **27**, 24 (2022).
3. N. D. Merner *et al.*, Arrhythmogenic right ventricular cardiomyopathy type 5 is a fully penetrant, lethal arrhythmic disorder caused by a missense mutation in the TMEM43 gene. *Am. J. Hum. Genet.* **82**, 809-821 (2008).
4. B. Baskin *et al.*, TMEM43 mutations associated with arrhythmogenic right ventricular cardiomyopathy in non-Newfoundland populations. *Hum. Genet.* **132**, 1245-1252 (2013).
5. M. W. Jang *et al.*, A nonsense TMEM43 variant leads to disruption of connexin-linked function and autosomal dominant auditory neuropathy spectrum disorder. *Proc. Natl. Acad. Sci. U. S. A.* **118** (2021).
6. H. Milting *et al.*, The TMEM43 Newfoundland mutation p.S358L causing ARVC-5 was imported from Europe and increases the stiffness of the cell nucleus. *Eur. Heart J.* **36**, 872-881 (2015).
7. V. Siragam *et al.*, TMEM43 mutation p.S358L alters intercalated disc protein expression and reduces conduction velocity in arrhythmogenic right ventricular cardiomyopathy. *PLoS One* **9**, e109128 (2014).
8. L. Bengtsson, H. Otto, LUMA interacts with emerin and influences its distribution at the inner nuclear membrane. *J. Cell Sci.* **121**, 536-548 (2008).
9. M. W. Jang *et al.*, A Deafness Associated Protein TMEM43 Interacts with KCNK3 (TASK-1) Two-pore Domain K(+) (K2P) Channel in the cochlea. *Exp. Neurobiol.* **30**, 319-328 (2021).
10. J. B. YinHua Zhang, HoKyung Sung, SangHyun Lee, Shin Young Ryu, Suk-Ho Lee, Won-KyungHo and Yung E. Earm, Stretchactivated and background nonselective cation channels in rat arterial myocytes. *Journal of Physiology* **523.3** (2000).
11. Y. Horio *et al.*, Clustering and enhanced activity of an inwardly rectifying potassium channel, Kir4.1, by an anchoring protein, PSD-95/SAP90. *J. Biol. Chem.* **272**, 12885-12888 (1997).
12. C. A. t. Taylor *et al.*, OSR1 regulates a subset of inward rectifier potassium channels via a binding motif variant. *Proc. Natl. Acad. Sci. U. S. A.* **115**, 3840-3845 (2018).
13. C. B. Ransom, H. Sontheimer, Biophysical and pharmacological characterization of inwardly rectifying K+ currents in rat spinal cord astrocytes. *J. Neurophysiol.* **73**, 333-346 (1995).
14. S. E. Nwaobi, V. A. Cuddapah, K. C. Patterson, A. C. Randolph, M. L. Olsen, The role of glial-specific Kir4.1 in normal and pathological states of the CNS. *Acta Neuropathol.* **132**, 1-21 (2016).
15. B. Djukic, K. B. Casper, B. D. Philpot, L. S. Chin, K. D. McCarthy, Conditional knock-out of Kir4.1 leads to glial membrane depolarization, inhibition of potassium and glutamate uptake, and enhanced short-term synaptic potentiation. *J. Neurosci.* **27**, 11354-11365 (2007).
16. M. M. S. George Liapakis, Jonathan A. Javitch, The Substituted-Cysteine Accessibility

Method (SCAM) to Elucidate Membrane Protein Structure. *Current Protocols in Neuroscience* **8**, 4.15.11-14.15.10 (2001).

17. I. M. Skerrett *et al.*, Application of SCAM (Substituted Cysteine Accessibility Method) to Gap Junction Intercellular Channels. *Cell Communication & Adhesion* **8**, 179-185 (2009).
18. G. Stelzer *et al.*, In-silico human genomics with GeneCards. *Hum Genomics* **5**, 709-717 (2011).
19. Y. D. Yang *et al.*, TMEM16A confers receptor-activated calcium-dependent chloride conductance. *Nature* **455**, 1210-1215 (2008).
20. G. S. Hong *et al.*, Tentonin 3/TMEM150c Confers Distinct Mechanosensitive Currents in Dorsal-Root Ganglion Neurons with Proprioceptive Function. *Neuron* **91**, 107-118 (2016).

Figure 1

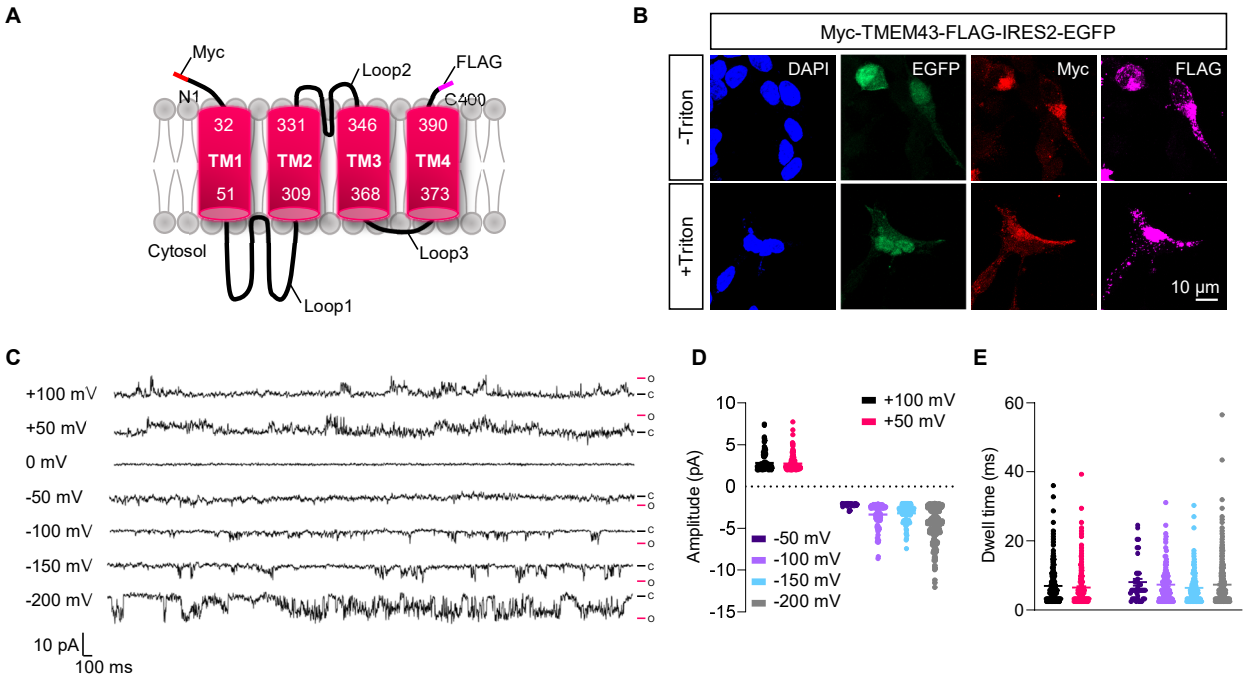

Figure 2

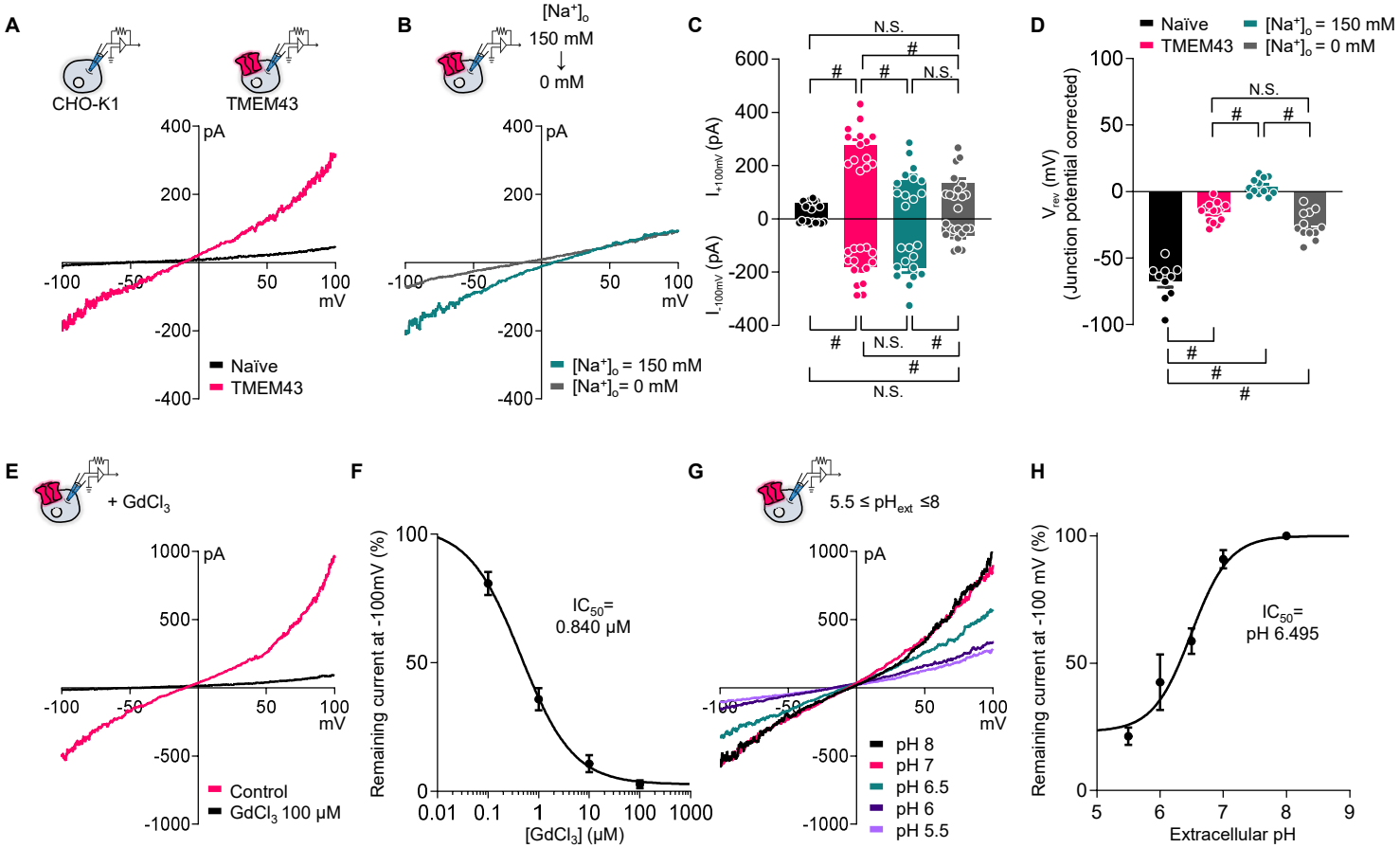

Figure 3

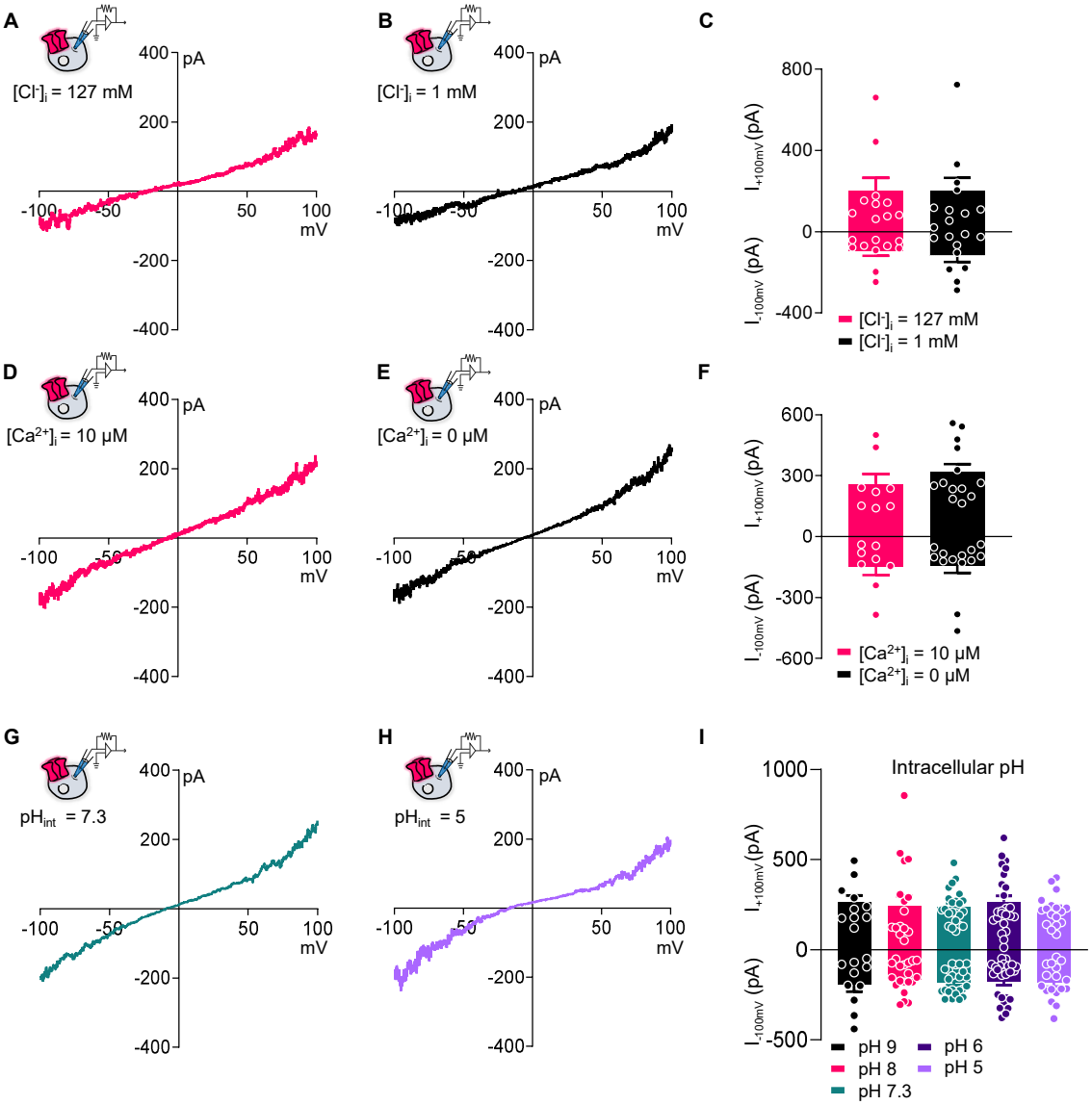

Figure 4

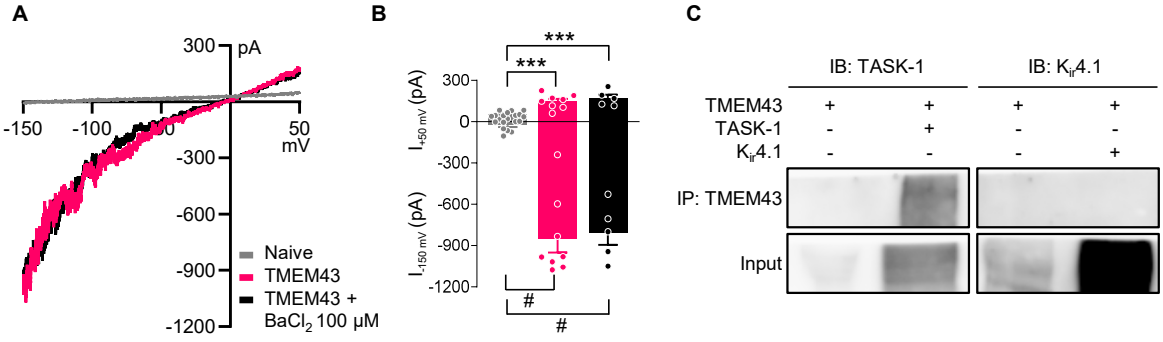

Figure 5

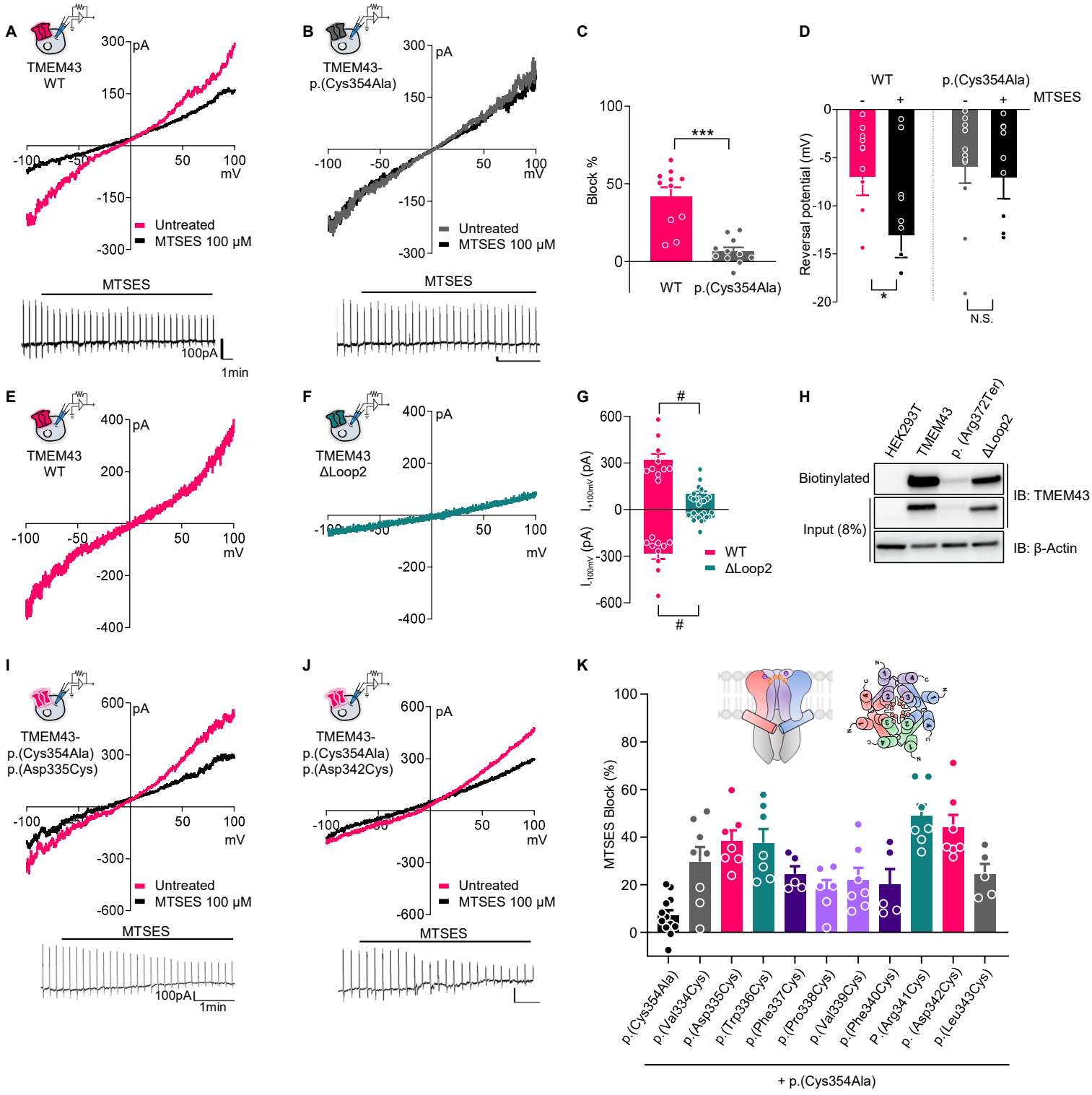

Figure 6